Fear and foraging in the ecosystem size spectrum generate diversity in fish life histories

Kindsvater, Holly K.[1], Juan-Jordá, Maria-José[2,3], Dulvy, Nicholas K.[2], Horswill, Cat[4,5,6], Matthiopoulos, Jason[7], Mangel, Marc[8,9]

1. Dept. of Fish and Wildlife Conservation, Virginia Polytechnic Institute and State University, 310 W. Campus Dr., Blacksburg, VA 24061, USA
2. Earth to Ocean Research Group, Dept. of Biological Sciences, Simon Fraser University, Burnaby, BC V5A 1S6 Canada
3. AZTI, Marine Research, Basque Research and Technology Alliance (BRTA). Herrera Kaia, Portualdea z/g, 20110 Pasaia – Gipuzkoa, Spain.
4. ZSL Institute of Zoology, Regent's Park, London, NW1 4RY, UK
5. Centre for Biodiversity and Environmental Research, Department of Genetics, Evolution and Environment, University College London, Gower Street, London, WC1E 6BT, UK
6. Department of Zoology, University of Cambridge, Downing St, Cambridge CB2 3EJ, UK
7. Institute of Biodiversity, Animal Health and Comparative Medicine, Graham Kerr Building, University of Glasgow, Glasgow, G12 8QQ, Scotland.
8. Theoretical Ecology Group, Dept. of Biology, University of Bergen, Bergen 5020, Norway
9. Institute of Marine Sciences and Dept. of Applied Mathematics and Statistics, University of California, Santa Cruz, CA 95064, USA.

Abstract

Understanding how changing environmental conditions affect fish growth and reproduction is critical to predict the consequences of climate change, yet studies focused on the physiological effects of temperature upon life histories often ignore size-dependent foraging and risk of predation. We embedded a state-dependent energetic model in an ecosystem size spectrum model to characterize prey availability (foraging) and risk of predation (fear) experienced by individual fish as they grow. We examined how spectrum richness and temperature interact to shape growth, reproduction, and survival; we found that richer spectra led to larger body sizes, but effects of temperature on body size were small. We applied our model to scenarios corresponding to three ecological lifestyles (ecotypes) of tunas, in some cases including seasonal variation in conditions. We predicted realistic estimates of growth and body sizes of tunas and found that seasonality in resources and temperature could lead to giant body sizes (> 300 cm), due to the compression of reproduction into shorter timeframes. Our framework for predicting emergent life histories combines direct and indirect effects of productivity (foodscapes), individual risk (fearscapes), and metabolic processes. This approach can be used to reconcile disparate results on fish life history responses to changing ocean conditions.

Keywords – Body size evolution, energy budgets, metabolic theory, size spectra, state-dependent models, temperature-size rule, global climate change

Introduction

Correlations between increased temperature and decreased body size have been documented for a variety of species (Gillooly et al. 2001, Kingsolver and Huey, 2008). The body sizes and population biomasses of aquatic species are responding strongly and rapidly to human-induced environmental change (Oke et al. 2020), motivating the need for biophysical models to explain these patterns (Cheung et al. 2008, Cheung et al. 2010, Blanchard et al. 2012, Fernandes et al. 2020). Yet not all aquatic species are responding in the same way to increased temperatures, resulting in winners and losers in abundance and average body size (Free et al. 2019, Audzijonyte et al. 2020). Beyond thermal physiology, the ecological and evolutionary mechanisms driving body size in the ocean remain poorly understood (Daufresne et al. 2009, Audzijonyte and Richards 2018, Neubauer and Andersen 2019). We hypothesize that this is because the demographic consequences of changing ecosystem productivity (foodscapes) and predator abundance (fearscapes) are difficult to disentangle from the direct effects of environmental temperature and its seasonality.

Research on life-history evolution has shown that within ectothermic species, both increased risk of predation and food availability can select for earlier ages at maturation and faster growth, resulting in smaller body sizes (Conover and Munch 2002; Walsh and Reznick 2009). Within and between species, development at hotter temperatures can lead to smaller body sizes (Kingsolver and Huey 2008). By contrast, there are few predictions for the role of seasonality in resource availability or temperature on growth in ectothermic organisms such as fishes, although polar regions are known to harbor larger individuals in terrestrial environments (Varpe 2017). Understanding the interactions between predation risk, resources, and temperature, including

seasonality in these processes, requires models that combine known relationships between fitness and body size, the rate of mortality, and energy availability to predict growth, body size, and reproduction.

The search for such mechanistic "rules" that link traits and communities can be traced to fundamental ecological theory (Charnov and Krebs 1974, Southwood 1977, Charnov et al. 1991, Gislason et al. 2010) , which predicts that intrinsic trade-offs connect life-history traits and determine individual body sizes and population demographic rates (Beverton and Holt 1959, Gadgil and Bossert 1970, Kozlowski, 1996). Since then, more detailed models of dynamic energy budgets have linked variable environmental conditions in time and space to fish growth and reproduction (Jorgensen and Fiksen 2006, Chapman et al. 2011, Audzijonyte and Richards 2018). Increasing attention has been paid to metabolic requirements (Jørgensen et al. 2016, Wong et al. 2021), which vary with the environmental temperature experienced by organisms (Brown et al, 2004, Clarke and Johnston, 1999). The allometric scaling of metabolic costs in different temperature regimes (known as the Metabolic Theory of Ecology [MTE]; Gillooly et al. 2001, Wong et al. 2021) has been used to predict that individual body sizes depend on the benefits of growing large (to increase foraging success and avoid predation), balanced against the costs of increased metabolic overhead and diverting resources from reproduction to growth. However, such general predictions struggle to explain latitudinal and temporal trends in body size within and among species of fish (Audzijonyte et al. 2020), suggesting that simplistic models do not sufficiently capture the relevant physiological and ecological drivers of fish life histories.

We hypothesize that accounting for community interactions, in addition to temperature, could explain diversity in fish life histories and provide insights into the mechanisms that determine adaptive responses to changing environmental conditions. In aquatic ecosystems, size spectra relationships are often used to represent community interactions, as they connect body size, trophic level, and abundance across species (Sheldon et al. 1977, Thygesen et al. 2005, Law et al. 2009, Sprules and Barth 2016, Andersen et al. 2016, Andersen 2019). In a community size spectrum, flow of energy between trophic levels via consumption and predation rates are characterized by individual mass, instead of species' identity (Benoît and Rochet 2004, Blanchard et al. 2009, Andersen 2019). The key property of size spectra is that an individual's relative position (mass) determines both its prey field (foodscape) and its risk of predation (fearscape). Individuals are born small and grow through the size spectrum over their lifetime, consuming prey that are a fraction of their own size. Furthermore, size-spectrum theory assumes the lower limit of prey size preference depends on the profitability of the prey, and the upper limit depends on the maximum gape size of the predator. These interactions could equally apply to interactions within size-structured populations of the same species (i.e. cannibalism). Therefore, predation and consumption rates determined by different areas under a size-spectrum curve could be used to simultaneously characterize the mass-specific caloric resource availability (foodspace) and risk of predation (fearscape) experienced by an individual as it grows (Benoît and Rochet 2004, Andersen 2019).

Here, we predict the evolution of diverse fish life histories using an energetically based model combining size-dependent resources and risk of predation (both derived from size-spectra) with physiological requirements at different environmental temperatures. To do this, we develop a

novel framework combining community size-spectrum theory with energetic models of growth and reproduction, such that allocation in one month affects an individual's size, survival chances, and resources for reproduction in the next. We define fitness as expected lifetime reproductive success and determine its maximum value and the associated life history decisions using stochastic dynamic programming (Clark and Mangel, 2000, Houston et al.1988, Mangel, 2015). We then examine general patterns in the life history evolution for fishes under different scenarios of ecosystem productivity and environmental temperature. Furthermore, we use our framework to investigate the evolution of growth, body sizes and reproductive patterns in tuna species in varying environments, including seasonally varying conditions. Tunas (Family *Scombridae*) exhibit a wide range of maximum body sizes (~ 40cm - 400cm), longevities (~ 4 - 41 years) and reproductive patterns (Juan-Jorda et al. 2013, Horswill et al. 2019). Tunas are epipelagic species found in temperate and tropical waters around the world's oceans with varying vertical, latitudinal and seasonal distributions and movements. Validating our model's ability to predict the life history diversity observed in tuna species in different environmental conditions gives us insight into the mechanisms underlying fish life histories and improve our ability to predict their response to future climate scenarios.

Methods

Defining and using the size spectrum to infer per-mass rates of prey encounter and predation

Studies across many orders of magnitude find that the relationship between the numbers of organisms and individual mass w is a power function with a scaling parameter κ and an exponent λ (Sprules and Barth 2016, Hatton et al. 2021)

$$N(w) = \kappa w^{\lambda} \tag{1}$$

The biomass size spectrum is the distribution of total ecosystem biomass *B(w)* across body size classes, and is proportional to $B(w) = N(w)w$. Based on evidence from multiple ecosystems (Sprules and Barth 2016), total biomass slowly decreases as individual mass increases; the slope of this line is typically -0.05, so that in log-log space, the biomass size spectrum is nearly flat (Sheldon et a. 1972, Andersen 2019). We consider this index of biomass to reflect whole-ecosystem productivity. Prior research suggests that the phenomenon of linear aquatic size spectra emerges from three size-dependent eco-physiological processes: (1) the encounter rate of predators and prey; (2) the preference of predators for prey of a given size; and (3) the limit to prey consumption imposed by the size of the predator's stomach (the predator-prey mass ratio; Benoît and Rochet 2004, Blanchard et al. 2017, Andersen 2019).

Anderson (2019) derived a method to calculate the prey available to an individual of size *w* by relating the richness of a spectrum $B(w)$ to empirical estimations prey encounter rates, predator-prey mass ratios, and prey preferences. Following his rationale, we assume that the prey biomass available per month to an individual is a concave function of mass *w*, and scaled to be approximately three times the size spectrum productivity κ. Therefore, the per-period consumption for an individual of mass *w* is represented by

$$B_{prey}(w) = 3\kappa w^{-0.05} \tag{2}$$

This equation approximates the integral over the foodscape of prey biomass (in kg) available to an individual of size *w* each month (Fig. 1A). The foodscape is total biomass acquired by the predator, and the range of sizes of prey that it takes.

We define the fearscape as an individuals' instantaneous risk of predation, integrated across sizes of potential predators. For gape-limited taxa like fishes, a predator's prey field depends on its encounter rate with prey in its preferred size range. This encounter rate (the clearance rate) is typically measured in units of volume per time, as aquatic species forage in a three-dimensional habitat (Kiørboe and Hirst 2014). Again, we follow Andersen (2019), and use an empirically estimated constant of 0.07 to characterize the scaling of prey vulnerability with mass, given estimates of preference windows of predators and the volume of water each clears that come from empirical distributions of prey sizes in predator guts (Ursin 1973). We also define a coefficient *h,* which modifies the probability of consumption - how likely a predator is to capture the focal individual (based on its hunger level or capture efficiency) - and use the reported allometric exponent of -0.25 to represent how consumption scales with body size (Figure 1B; Andersen 2019). From these, the integrated foodscape gives us the instantaneous mass-specific rate of mortality of prey $\mu_p(w)$ per month:

$$\mu_p(w) = 0.07hw^{-0.25} \tag{3}$$

We convert this instantaneous rate to the probability escaping from predators during each month (Hilborn and Mangel 1997, Mangel 2006), so we can represent the probability an individual of mass *w* surviving from one month to the next as:

$$\gamma_{pred}(w) = e^{-\mu_p(w)} \tag{4}$$

Defining physiological costs that depend on temperature and body mass

We assume metabolic costs that increase with body mass and environmental temperature (Clarke 2006). We model mass-dependent costs $C(w,\tau)$ (in joules) as a function of temperature τ in Kelvin, following the general form introduced in the MTE (Gillooly et al. 2001). Evidence for the MTE suggests the activation energy E (the energy required for the reactions of respiration and other metabolic processes) does not vary appreciably among taxa (Bernhardt et al. 2018); Boltzmann's constant k_B also does not vary. The normalization coefficient c accounts for differences among taxonomic groups in the intercepts of the linear relationship that arise from second-order effects such as stoichiometry or respiratory surface areas (Bigman et al 2021). The slope of this relationship in log space, θ, is strikingly similar among taxa (Brown et al. 2004). Note that τ in Eq. 5 is Kelvin, but hereafter we discuss temperatures in units of Celsius. The general form is:

$$C(w,\tau) = cw^{\theta} e^{\left(-E/k_B\tau\right)} \tag{5}$$

We use this general formula for scaling of metabolic costs at different temperatures τ to describe the monthly energetic expenses of an individual of mass w (Fig 1C).

201

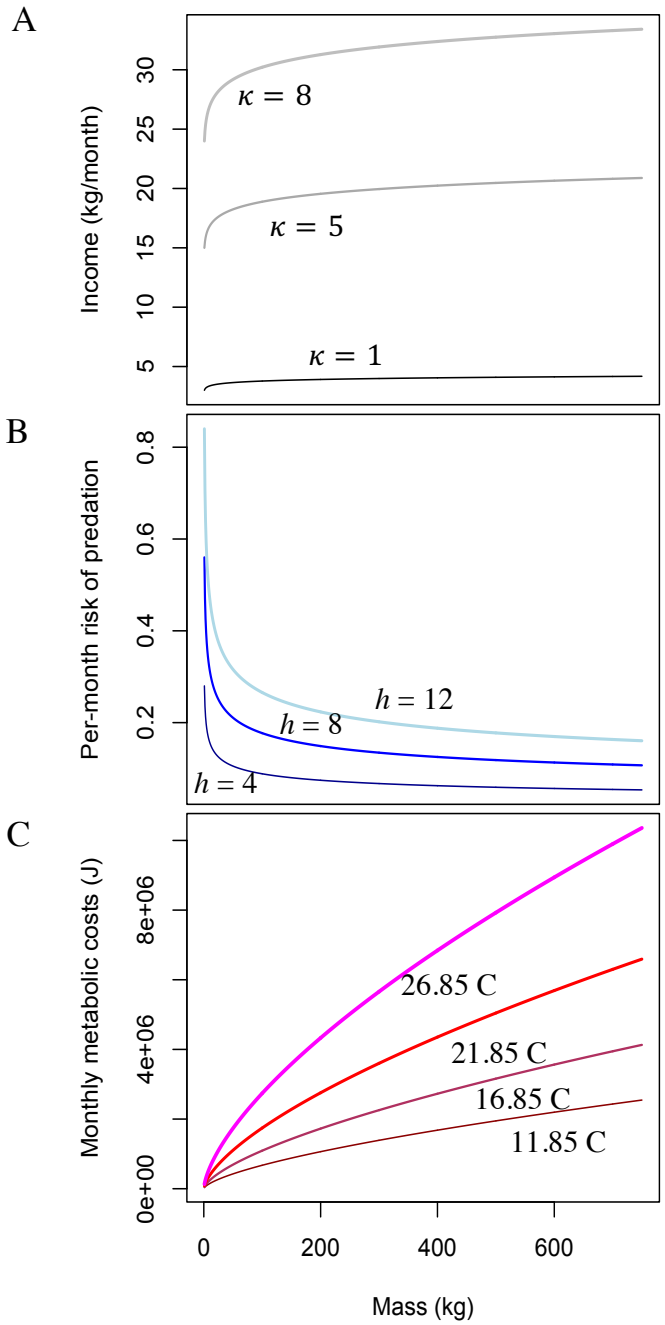

Figure 1. Examples of allometric relationships between individual mass and (A) income (in kg per month); (B) the scaling of predation with size and its interaction with predator efficiency (or hunger) h, and (C) metabolic costs, which also scale with temperature τ (on the graph, it is presented in degrees Celsius, C). Note that these curves represent a sample of values considered, but we also considered values outside these ranges where specified.

Defining fitness and determining the optimal allocation strategy

In Equations 2, 4, and 5, we define mass-specific food availability, costs, and predation risk, allowing us to examine the variables influencing growth and reproduction in a common currency of an individual's energy budget (Fig. 1). To find the optimal life history strategy in different scenarios of ecosystem productivity and temperature conditions, including seasonal variation, we developed a model of an individual's energy budget, tracking two physiological state variables, the length and energy (lipid) stores of an individual, which vary dynamically over an individual's lifetime (Fig. 2). Following the conventions for dynamic state-variable models, we denote the state variables l and s are lowercase in the dynamic programming equation, representing the fact they are iterated values. Later, when we refer to specific values of the state variables, we use uppercase L and S.

We define fitness as lifetime reproduction, expected over the stochastic process of survival, which we calculate numerically using stochastic dynamic programming (Houston et al. 1988; Clark and Mangel 2000, Mangel, 2015). This method allows us to consider how individual age and physiological state (energy stores and body length) affect the optimal trade-off between growth and reproduction in the context of lifetime fitness. We assume that an individual allocates a proportion of its budget to growth and reproduction on monthly time intervals. Our choice to model allocation to growth and reproduction as proportions of an individual's energy budget builds on prior dynamic state-variable models of fish growth (Jørgensen and Fiksen 2006, Chapman et al. 2011).

Given specific values of $L(t)$ and $S(t)$, representing individual length and stores at the start of month *t,* we calculate structural mass $W(t)$ from length with a standard cubic function (Froese 2006):

$$W(t) = aL(t)^3 \tag{6}$$

and assume that only structural mass is relevant for size-dependent gains (B_{prey}) and costs (Fig. 2). We convert from mass to units of energy (joules) and back using the conversion factor $\rho = 4.2 \times 10^6$J/kg (Chapman et al 2011). Each month, an individual acquires energy from food, determined by their structural mass *w* via Eq. 2. We then allow the individual to allocate proportions of its energy budget (which includes income and any stored energy) to growth (*g*) and reproduction (*r*).

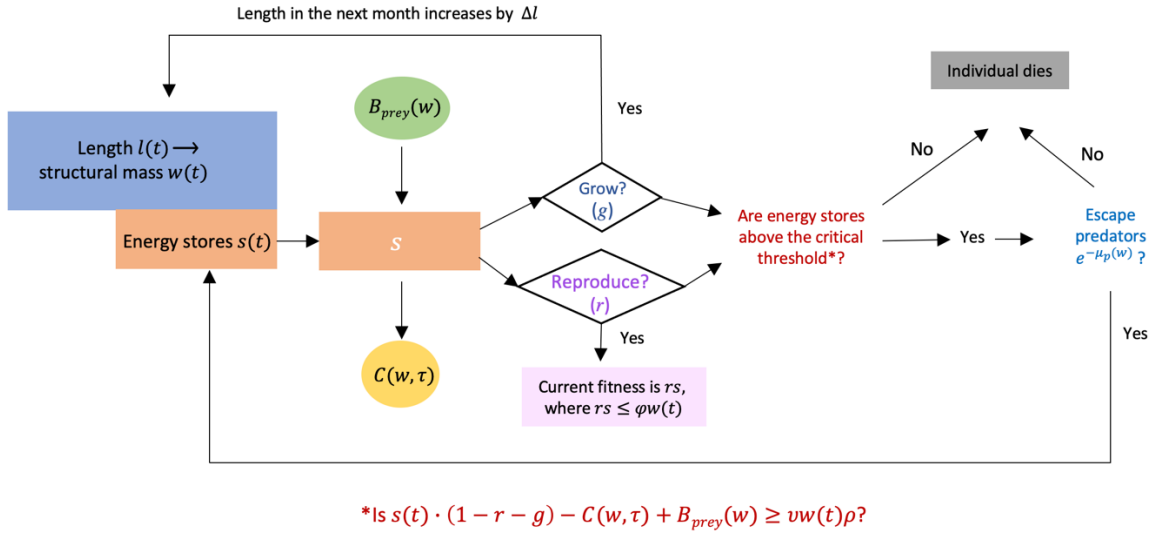

Figure 2. Schematic overview of the optimization algorithm calculating the two dynamically varying state variables, length $l(t)$ and energy stores $s(t)$ within each month t, as well as current and expected fitness. Round shapes represent inputs; rectangular shapes are model states and outputs (fitness and fate); diamonds are decisions. Note that $l(t)$ and $w(t)$ are related through Eq. 6. Both B_{prey} and μ_p are determined by the size spectrum. Survival to the next time step depends on (1) whether there is sufficient energy to allocate to growth and reproduction, pay costs, and exceed the critical threshold for lipid stores, and (2) the size-dependent risk of predation μ_p.

Given an individual of with specific values for length $L(t)$ and energy stores $S(t)$, we can calculate the increment of growth ΔL expected for each possible proportional allocation g. We convert this fraction of lipid stores from joules to the equivalent mass ($g\frac{S(t)}{\rho}$), and add it to

existing mass, such that $W(t+1) = W(t) + g\frac{S(t)}{\rho}$. We then calculate the new length by rearranging the mass-length relationship $W(t) = aL(t)^3$:

$$L(t+1) = \left[\frac{1}{a}\left(L(t)^3 + g\frac{S(t)}{\rho}\right)\right]^{1/3} \tag{7}$$

We repeat this for every possible combination of values of the state variables, *l* and *s.* For all $L(t) = l$ and $S(t)$ = s, we can determine the growth increment ΔL:

$$\Delta L(l, s, g) = \left[\frac{1}{a}\left(l(t)^3 + g\frac{s(t)}{\rho}\right)\right]^{1/3} - l \tag{8}$$

Values for proportional allocation of lipid stores to reproduction *r,* along with *g,* are combined to determine the dynamics of energy stores and length from one month to the next:

$$S(t+1) = B_{prey}(W(t)) - C(W(t), \tau) - (r+g) \cdot S(t)$$

$$L(t+1) = L(t) + \Delta L(L(t), S(t), g) \tag{9}$$

We assume that both stored energy and reproduction are limited by an individual's structural mass (which in turn depends on its length). These constraints represent limits on the amount of lipid that it is realistic to store, and mass of gametes that can be produced, given the capacity of the body cavity. If the proportions of energy allocated to reproduction and growth are less than 100% (meaning $r + g < 1$), the remaining energy is stored for future use, as long as total reserves do not exceed 60% of structural mass. This value is somewhat arbitrary but exploratory analyses suggest it does not have a strong effect on the results presented here because in practice individuals only store enough energy to ensure their critical threshold is met. Second, we assume

that reproductive output (in units of kg) is constrained so that it cannot exceed a fixed proportion of φ of structural mass $w(t)$, so that the following condition must be met:

$$\frac{rS(t)}{\rho} \leq \varphi w(l,t) \tag{10}$$

This size-based limit on total reproduction is used in the calculation of current fitness.

Current fitness

We let $R(r,s,l,t)$ denote the increment in fitness in month *t* when $L(t) = l$, $S(t) = s$, and a fraction of stores *r* is allocated to current reproduction. Note that when $\varphi w(l,t) >> \frac{rs}{\rho}$, $R(r,s,l,t) \sim rs$ and when $rs >> \varphi w(l,t)$, then $R(r,s,l,t) \sim \varphi w(l)$. We model this constraint with an asymptotic function, such that the fitness increment increases smoothly toward the maximum possible for the given length *l(t).* This relationship is defined as

$$R(r,s,l,t) = \frac{rs}{1+({rs}/{\varphi w(l)})^f} \tag{11}$$

The asymptotic value of this function depends on the value of *f* in the denominator, which controls the abruptness of the constraint on current fitness (Supp. Fig. 1). In other words, the steepness of the multivariate landscape around the fitness optima is modulated by *f.* For simplicity, we assume $f = 1$ for all results presented hereafter.

Expected future fitness

To calculate future fitness, we calculate the future states (length and lipid stores) given each combination of allocation to growth and reproduction. We denote potential values of future states as $l'$and s'. In light of Eqs 7-11 these are

$$l'(l,s,g) = l + \Delta l(l,s,g)$$

$$s'(l,s,r,g) = B_{prey}\big(w(l)\big) - C(\,w(l),\tau) - (r+g)s \qquad (12)$$

where $w(l)$ is the structural mass of an individual of length *l.* At the end of the month, if an individual's lipid stores fall below the critical threshold for its mass (its expenditures have exceeded its energy budget), it starves (Supp. Fig. 2). We let $\gamma_s(s,l)$ denote the probability of avoiding starvation in the current time and model it as

$$\gamma_s(s,l) = \frac{1}{1+e^{-q(s-\upsilon w(l)\rho)}} \qquad (13)$$

involving two new parameters *v* and *q*. The parameter *v* determines the level of stores at which starvation begins and q is a shape parameter. When $s = \upsilon w(l)\rho$, the right-hand side of Eq. 13 is always ½. When q is large, then the right-hand side of Eq. 13 is approximately 1 when $s > \upsilon w(l)\rho$ and 0 otherwise. Thus, this function specifies that if combined allocation to growth and reproduction causes an individual's lipid stores to decrease below the critical value for its mass the probability of survival decreases smoothly toward zero (See Supp. Fig. 2 for more details).

Equation 7-13 characterize changes in individual state and in fitness, given the possible monthly allocation strategies (*r* and *s*). With these functions in place, we can find the allocation strategy

that maximizes current and future fitness at every age until the age of senescence or maximum lifespan, T, is reached (for all scenarios, we assumed the maximum lifespan of T = 216 months or 18 years). We define $V(l, s, t)$ as the maximum expected accumulated reproduction between time t and T, for all possible values of the state variables (size $L(t) = l$ and lipid stores $S(t) = s$). Since there can be no accumulated reproduction after T, we have the end condition $V(l, s, T) = 0$. Expected future fitness at every age $t < T$ is found by solving the stochastic dynamic programming equation

$$V(l, s, t+1) = \max_{g,r}\left[R(r, l, s, t) + \gamma_{pred}(w) \cdot \gamma_s(s, l) \cdot V\big((l'(l, s, g), s'(l, s, r, g), t\big)\right] \qquad (14)$$

The first term of the on the right-hand side of Eq. 14 represents reproduction in month t. The second term represents expected future reproduction, discounted by the probability of begin eaten $\gamma_{pred}\ (w)$or starving $\gamma_{pred}(w)$, When these are combined, we obtain expected lifetime reproduction from time t onwards, given that size $L(t) = l$ and lipid stores $S(t) = s$. The dynamic programming algorithm (Mangel and Clark 1988; Houston and MacNamara 1999) iterates over all viable combinations of l and s, at each time t, and stores the fitness of each allocation strategy. The optimal strategy at time t is the combination of g and r associated with the greatest current and future fitness. Further details of the optimization algorithm are given in the Appendix. Figure 3 depicts the array for both allocation strategies ($g^*(l,s,t)$ and $r^*(l,s,t)$) at two ages, for all possible combinations of length and lipid stores.

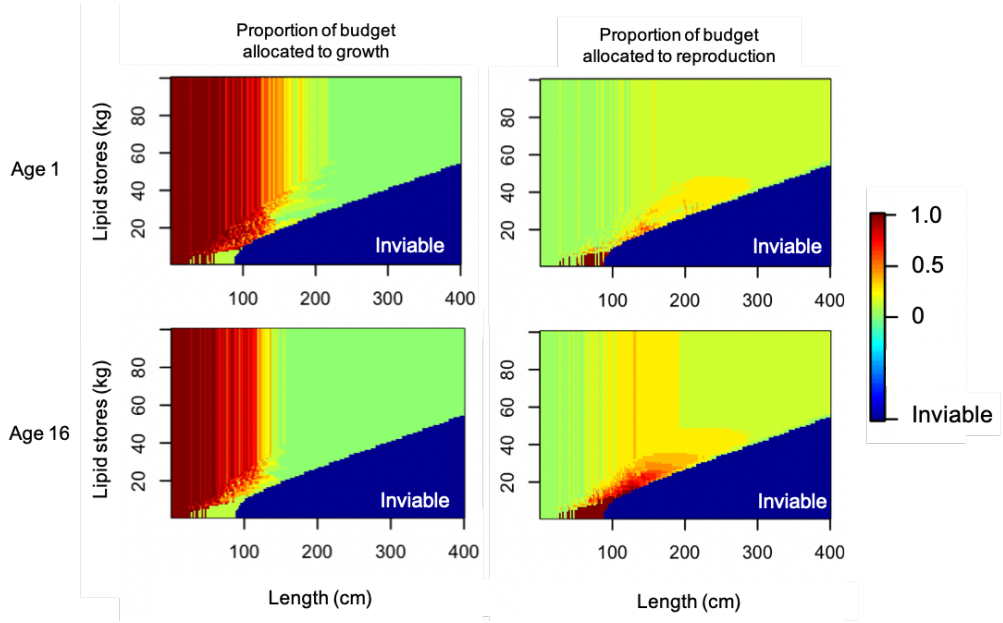

Figure 3. Example rules for allocation to growth and reproduction for ages 1 and 16. The inviable region (dark blue) represents parameter space where remaining stores are insufficient for survival, given the individual's length (in other words, energetic requirements for maintenance are not met). Comparing panels within rows shows differences between allocation to growth and reproduction as a function of state and length. Comparing panels within columns shows how allocation to growth and reproduction, respectively, changes with age. Note that the striations come from the discretization of allocation values of g and r in Eq. 14.

Calculating the fate of individuals allocating optimally

We used a probabilistic approach to calculate the accumulating chance of mortality as an individual ages, following the allocation rules generated by the solution of Eq. 14, which provides optimal allocation rules for the range of state values specified in our numerical algorithm. Some combinations of states (length, lipid stores and age) will not arise naturally and

335 others are inviable (the dark blue regions of Fig. 3). Therefore, to predict the relationships
336 between length, lipid stores, and age that will be observed in nature, we simulate the expected
337 fates of an individual that is born at a given size, and allocates energy according to the optimal
338 growth and reproduction fractions given by the solution to Eq. 14. We record the body length
339 and reproductive output in each subsequent month of an individual's life, and calculate its
340 probability of survival, given both the risk of starvation and the risk of predation. We use the age
341 past which the cumulative chance of survival is less than 5% as the expected lifespan. For
342 simplicity, we consider reproductive output in units of energy (joules) rather than considering
343 allocation to offspring size and number (Kindsvater et al. 2010). We did not build in any
344 assumptions about age at maturation, but rather let maturation patterns emerge from patterns of
345 allocation to reproduction.
346
347 *Scenarios for environmental variation*
348 We used our model to predict a range of fish life histories (growth, reproduction, and survival)
349 that are evolutionarily advantageous across different scenarios of ecosystem productivity and
350 environmental temperatures. To do this, we developed different productivity and temperature
351 scenarios corresponding to different conditions in the marine environment, and impose different
352 metabolic costs to individuals according to Eq. 5. We solved for the optimal life histories under
353 different temperatures (τ in Eq. 5 in units of Kelvin), converted to Celsius and ranging from
354 11.85 to 26.85^{o}C (285-300 K), and under different scenarios for ecosystem productivity, for
355 which κ ranged from one to ten. There is very little information on how temperature and
356 ecosystem productivity are related in the ocean; therefore we considered all combinations of

these parameters to understand the implications of their interactions for the evolution of fish life histories.

Case study predicting life history diversity of tunas (Scombridae).

We developed a case study for tunas to examine if our model can predict the observed patterns of life history variation in tunas. There are 15 species of tunas (Family *Scombridae*, genera *Allothunnus*, *Auxis*, *Euthynnus*, *Katsuwonus*, *Thunnus*). These species inhabit a wide range of environmental conditions in marine ecosystems. Tuna species can be found in coastal and oceanic pelagic waters, and have wide geographic distributions, ranging from the tropics to higher temperate latitudes with some degree of habitat partitioning by depth. Tropical tuna species can spawn throughout the year, while the subtropical and temperate tunas undergo seasonal migrations back to warm waters for spawning (Juan-Jorda et al 2013, Horswill et al 2019). Paleoceanographic evidence suggests that ancestral tunas evolved in a tropical environment approximately 60 million years ago (Monsch 2000) and over time they have diversified and evolved a suite of morphological and physiological adaptations that have allowed them to expand their distributions into more temperate environments or deeper colder waters where they can encounter higher prey densities to support their high somatic and gonadal growth rates (Dickson and Graham 2004). Reflecting their tropical ancestor, all tunas (except for the slender tuna *Allothunnus fallai*) spawn in warm waters with a sea surface temperature of at least 24 ^{o}C (Schaefer 2001).

380 To connect our mechanistic model more explicitly with the observed patterns of life history
381 variation in tunas, we followed a proposed categorization of tunas into three ecological lifestyles,
382 (Bernal et al. 2017). The three general lifestyles are based on species-specific vertical,
383 latitudinal, and temporal (seasonal) distributions and movement patterns of tunas (Fig. 4; Bernal
384 et al. 2009, Bernal 2011, Bernal et al. 2017). The first ecological lifestyle represents a tuna
385 species that largely remain within the warmer and well-oxygenated surface layer above the
386 thermocline (generally above 20 ºC) during both day and night. These tuna species have limited
387 vertical movements as they do not descend below the thermocline (Figure 4). Coastal species,
388 such as the tropical frigate tuna *(Auxis thazard)* may typify this group. The second ecological
389 lifestyle represents tuna species that spend the majority of the time above the thermocline
390 (generally above 20 ºC) but also visit depths below the thermocline for foraging (Figure 4). The
391 oceanic species of yellowfin tuna (*Thunnus albacares*) with year-round tropical distributions
392 may typify this group. Its vertical movement exposes this species to a wider range of
393 temperatures and to less-oxygenated waters at depth but only for short periods of time because
394 this species is not hypoxia tolerant (Schaefer et al. 2009). The third ecological lifestyle
395 characterizes tuna species that are exposed to a wider range of environmental conditions and
396 spend significant periods of time in colder waters (Figure 4). The oceanic and temperate Atlantic
397 bluefin tuna (*Thunnus thynnus*) are one species that typifies this group, spending most of the year
398 at higher latitudes in colder and more productive waters between the upper mixed later and the
399 cooler deep waters below the thermocline, and migrating to warmer waters for spawning (Bernal
400 et al. 2017).
401

To examine whether our model could predict the three broad ecological lifestyles of tunas, we defined three corresponding environmental scenarios for temperature, ecosystem productivity, and seasonality. For the first ecological lifestyle of tunas, we assumed individuals experienced average temperatures of 21.85 ^{o}C year-round and the low, stable productivity (κ =1) characteristic of the tropical warmer upper water mixed layer (most prey will be inaccessible below the thermocline). For the second ecological lifestyle, we again assumed constant temperature of 21.85 ^{o}C year-round but intermediate productivity (κ = 5) to represent the ability of individuals to undertake excursions of short duration below the thermocline for foraging. Finally, for the third ecological lifestyle, we assumed variable environmental temperature and productivity to capture seasonal latitudinal migrations. We assumed a temperature of 15 ^{o}C and a high ecosystem productivity value (κ = 12) for 9 months, representing conditions while individuals occur in colder high-latitude foraging grounds, and a temperature of 24 ^{o}C and lower ecosystem productivity (κ = 4) for 3 months, representing the period individuals are in the spawning grounds at lower warmer latitudes.

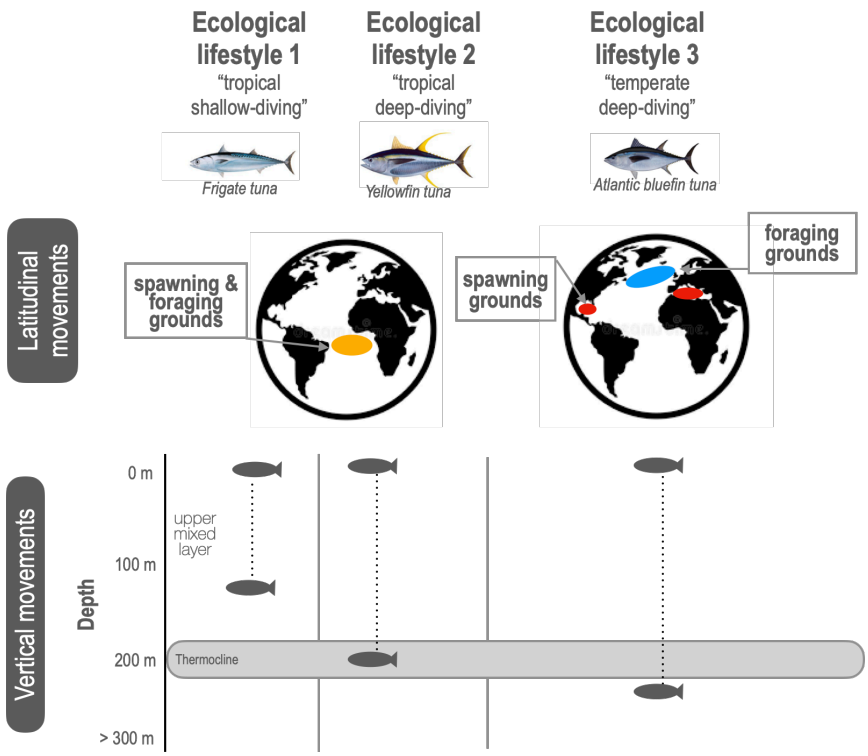

Figure 4. Three representative ecological lifestyles of tunas and their distribution patterns based on their latitudinal and vertical movements. Characteristic spawning and foraging grounds are shown for each lifestyle; examples are the tropical shallow-diving frigate tuna *Auxis thazard*, tropical deep-diving yellowfin tuna *Thunnus albacares,* and temperate deep-diving Atlantic bluefin tuna *Thunnus thynnus*. Fish silhouettes represent the depth distribution where species spend most of their time. The thermocline is defined as the depth range within which the water temperature changes rapidly and separates the water column into the upper well-mixed surface layer (water above 20 ºC) and the deeper waters (waters below 15 ºC). Figure modified from Bernal et al. 2009 and Bernal et al 2017.

Sensitivity analyses

We ran a series of tests to examine how our choices of parameters in the size spectrum influence model predictions. Specifically, we varied values of *h* (representing efficiency in prey capture or

hunger levels) in the predation function (Eq. 3) and φ (the fraction of body mass that can be devoted to reproduction) in the reproductive constraint (Eq. 10). In the tuna case study, we also varied the seasonal pattern of changes in environmental variables (expanding the warm season from three months to six months of the year) and allowed individuals to reproduce continuously (not just in restricted seasons) to understand the effects of seasonality in foraging and reproduction. We do not present formal analyses of the lower and upper limits on lipid stores, the shape and scale coefficients in Eqs. 2 and 3, nor c or θ in the metabolic cost function (Eq. 5) because preliminary exploration of our model indicated they had only minor effects on our model predictions. We infer this is because these parameters are all related to the scaling of available energetic income, physiological costs, and predation risk, and because they are all size-dependent in nature they have very similar effects to variation in κ (the size - spectrum coefficient, i.e., whole-ecosystem productivity, Eq. 1). We also determined in preliminary analyses that the maximum lifespan T did not strongly affect model results, because most individuals reach a maximum body size well before T and their energetic budget and predation risk do not change as the individual approaches T.

Results

Our model produces age-specific relationships between body size (length, from which we calculate mass using Eq. 6) and reproduction that correspond to a range of fish life histories. In general, we found that individuals allocated energy to growth early in life and shifted this allocation to reproduction in later life. An asymptotic growth pattern naturally emerged from the model, after a period of exponential growth early in life (Fig. 5A). Ecosystem productivity (κ)

alone generated a range of maximum body sizes, from less than 100 cm at low levels of productivity to well over 250 cm (Fig. 5A). Across scenarios of ecosystem productivity, the predicted trajectories for individual growth were identical in early life. However, growth slowed earlier in lower productivity environments (Fig. 5A). We also found the pattern of age-specific mortality was very similar in early life for all productivities κ, but that lifespan increased predictably as asymptotic body size increased (Supp. Fig. 4). For all life histories, allocation to reproduction began at very low levels sometime during the individual's second year (Fig. 5B) and increased steadily as the individual aged until it reached a maximum. Both the rate at which reproduction increased with size and the maximum reproductive output were consistently greater with increased ecosystem productivity (Fig. 5B).

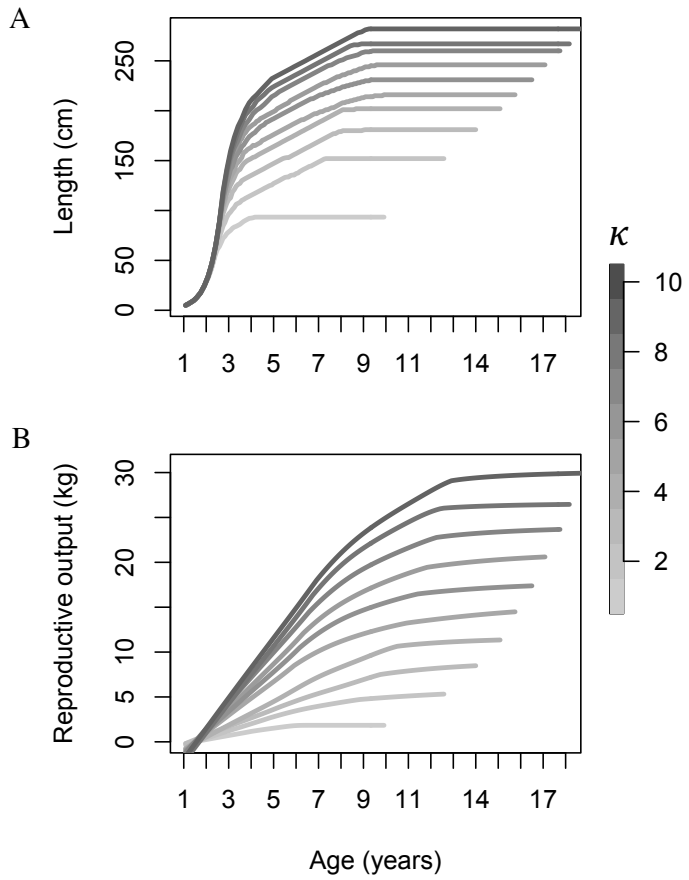

Figure 5. (A) Growth (size at age) and (B) Expected reproductive output of individuals in different productivity κ scenarios. Each curve ends when an individual's expected survival chances are less than 5%. Temperature in every scenario was constant at 16.85 ºC, and h was constant at 8. The reproductive output was smoothed using the lowess tool in R; raw data can be found in Supp. Fig 3.

When we compared the interacting effects of ecosystem productivity (κ) and environmental temperature (τ) on patterns of growth and reproductive allocation, we found the effects of temperature on body size and reproductive output were small (Fig. 6). This was especially true in low productivity scenarios, where only minor changes in body length emerged (Fig. 6A). In the warmest conditions (26.85 ºC), across all productivity scenarios, maximum body sizes were 5-10% smaller compared to the other temperature conditions (which ranged from 11.85 – 21.85 ºC). At higher productivity values ($\kappa > 5$), lifetime reproductive output decreased at warmer temperatures (Fig 6B). We infer the difference between low and high productivity environments for this result is due to larger body sizes and higher metabolic costs at higher temperatures.

Specifically, at higher temperatures, individuals reaching maximum lengths of more than 250 cm had a 5-8% reduction in lifetime reproductive output at º 26.85 C. This pattern suggests that large individuals can compensate for the increased metabolic demands in warmer conditions by reducing reproductive output.

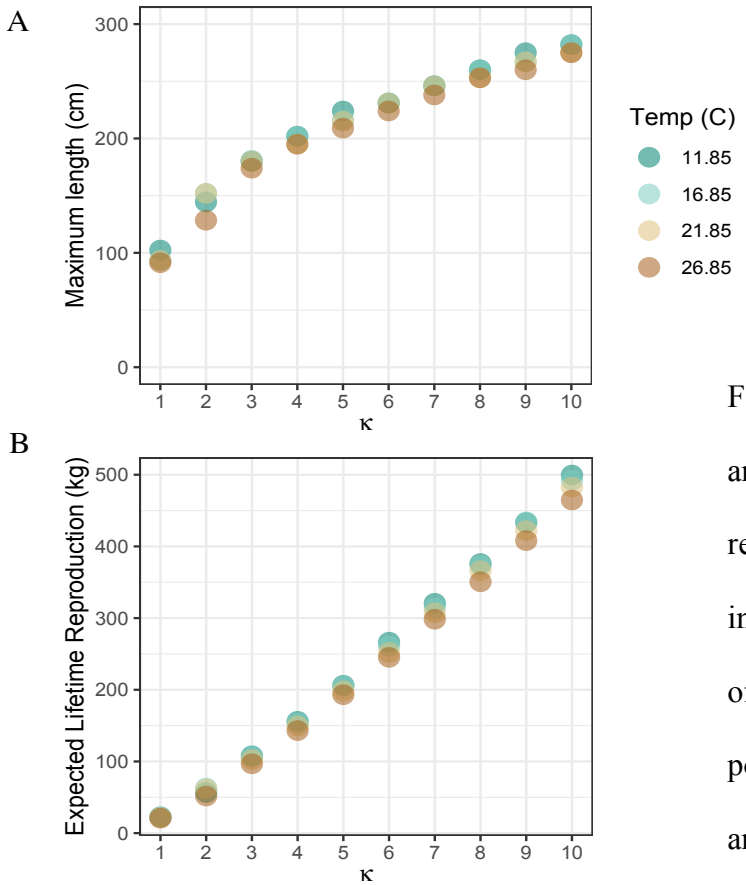

Figure 6. (A) Maximum body size and (B) Expected lifetime reproductive output (in kg) of individuals plotted against a range of productivity scenarios. Color of points corresponds to average annual temperature.

We found the effect of temperature on survival was indirectly expressed through body size, i.e., where temperature influenced asymptotic body size (Fig. 6A) it had a predictable effect on lifespan. Individuals reduced growth and remained smaller in thermally taxing conditions to avoid being unable to meet their energetic requirements for maintenance, which in our size-structured model equates to an increased risk of predation and thus shorter lifespans. In

477 sensitivity analyses we found the parameter *h,* representing predator efficiency or hunger level
478 (Eq. 3; Andersen 2019), changes the allometric properties of the risk of predation (Supp. Fig. 6).
479 However, while varying this parameter affected the realized lifespans, it did not dramatically
480 change individual growth trajectories or patterns of size-specific reproduction (Supp. Fig. 6).
481
482 *Case study of tunas*
483 When we compared the growth, body size, and reproductive patterns of tunas predicted by our
484 model in each of the three representative environmental scenarios (Figure 4), we found general
485 trends in life history that correspond to the representative species of each ecological lifestyle
486 (Figure 7). In the environmental scenario matching the tropical shallow-diving lifestyle, we
487 predicted individual body sizes of less than 100 cm. In this scenario, individuals were predicted
488 to mature between 2 and 3 years; less than 5% of individuals survived past 10 years of age and
489 they reproduced continuously at low levels (left column, Figure 7). This is consistent with the
490 life history of tropical shallow-diving tuna species (e.g. frigate tuna *Auxis thazard*). In the
491 environmental conditions matching the tropical deep-diving lifestyle, we predicted growth to
492 sizes of more than 200 cm, lifespans of less than 15 years, and continuous reproductive output
493 that increases over the individual's life (middle column, Figure 7); while we believe this is
494 consistent with the life histories of tropical deep-diving tuna species such as yellowfin tuna
495 *Thunnus albacares*, lifetime reproductive patterns of these batch-spawning species are not well
496 known (Horswill et al. 2019). For the lifestyle of temperate deep-diving tunas, we predict that the
497 maximum body sizes can exceed 300 cm; individuals live much longer than 18 years (right
498 column, Figure 7). Spawning was constrained to be seasonal in tunas in the third ecological
499 lifestyle (i.e., spawning could only occur in temperatures above 24 ^{o}C, which we specified for

three months of the year). We found that when environmental temperature and ecosystem productivity varied seasonally, individuals grew to be larger than three meters long; this is approximately 50 cm larger than the body sizes predicted under constant scenarios that are otherwise comparable in terms of productivity (κ) and temperature (τ) (Figures 5 and 6). As a consequence of foraging and reproduction each being compressed into seasons, for individuals with temperate, deep-diving lifestyles, monthly reproductive output dramatically exceeded that of other environments (note difference in y-axis scale in Figure 7F).

518

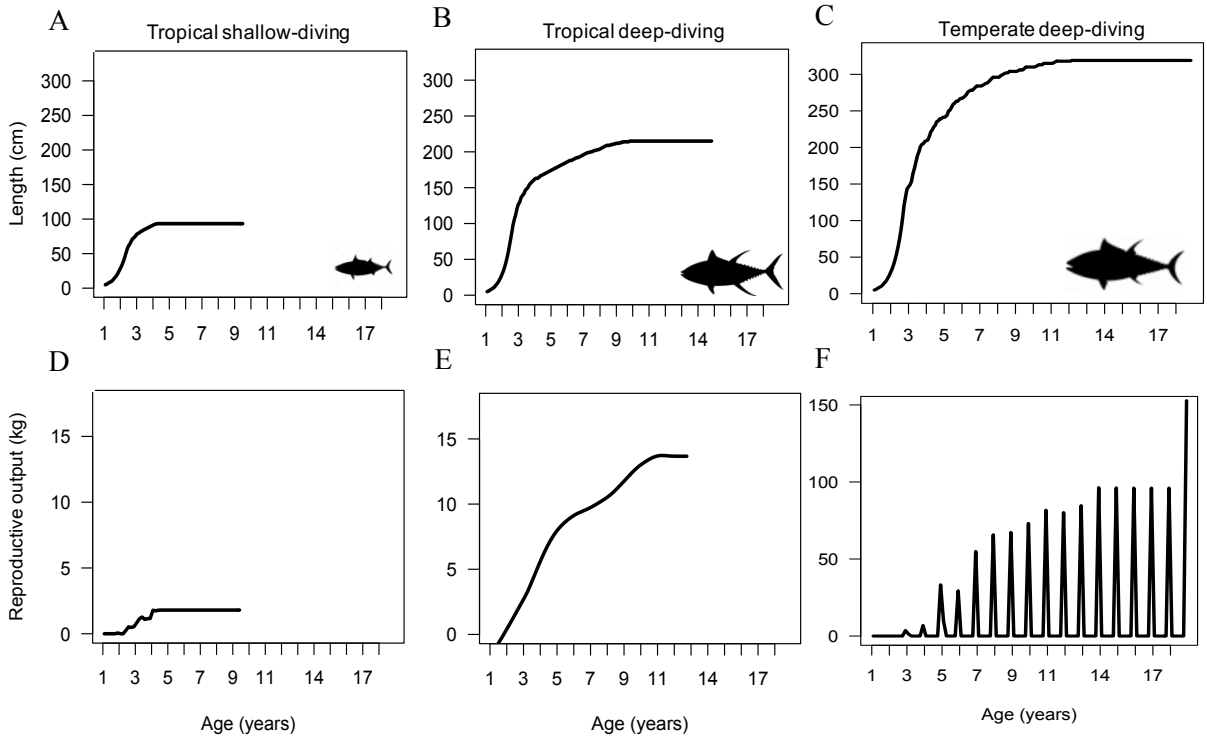

Figure 7. Growth (top row) and reproduction (bottom row) predicted by our model in each of the three representative environmental scenarios corresponding to the three ecological lifestyles of tunas (columns). As elsewhere, all curves end at the age when less than 5% of the population is expected to survive, representing the average lifespan of the individual. A and D represent tropical shallow-diving tuna species such as the frigate tuna *Auxis thazard*. B and E represent tropical deep-diving tuna species such as yellowfin tuna *Thunnus albacares*. C and F represent temperate deep-diving species such as Atlantic bluefin tuna *Thunnus thynnus*, which migrate seasonally from higher latitudinal colder and productive waters to less productive and warmer waters. Note that at age 18, around 6% of individuals in the temperate deep-diving lifestyle were still alive and likely could live much longer. As in Fig. 5, the reproductive output in panels D-F was smoothed using the loess function. Note that $h = 8$ for all scenarios.

The emergence of large body sizes in conditions corresponding to the temperate deep-diving lifestyle of tunas (Figure 7C) was robust to changes in the seasonal pattern of environmental variables and reproduction. To better understand the emergence of these giant individuals in seasonal environments, we considered an alternative scenario of seasonality in which individuals experienced only six months of cooler, richer ecosystem productivities and six months of warmer, poorer ecosystem productivities. We found the striking pattern of growth to large body sizes to be robust to these changes (Supp. Fig. 7). In fact, individuals actually achieved larger body sizes, suggesting that seasonality favors larger body sizes to increase the rate of uptake during the season of greatest resource abundance.

Discussion

Changes in environmental temperature and ecosystem productivity have been occurring for decades and have been shown to affect fish recruitment, growth, and fishery productivity (Free et al. 2019; Oke et al. 2020). There have been several mechanisms proposed to explain these changes (Fernandes et al. 2020). Early models based on physiology predicted that increased temperature will lead to reduced growth and smaller body sizes (Cheung et al. 2008), yet have been countered by recent experimental evidence showing growth is less affected by temperature than reproductive allocation (Wootton et al. 2022), and that metabolic rate can adapt to increased temperatures (Pilakouta et al. 2020). Physiological models have ignored ecological interactions because it has been challenging to represent and evaluate the effects of the food- and fearscape upon somatic growth. To address this gap, we developed a general model incorporating insights from size spectra theory to parametrize the risk of predation (fearscape) and the availability of

542 prey (foodscape) for individuals of different sizes. Our approach integrates community
543 processes, including size-specific foraging success and predation risk, into a model of individual
544 fitness. Our model predicted larger body sizes, greater reproductive output, and longer lifespans
545 when resources were plentiful; by contrast, in less productive ecosystems, individuals were
546 small, with shorter lifespans. The novelty of our results is that we were able to predict emergent
547 body sizes and reproductive and mortality rates mechanistically, without imposing invariant
548 relationships between growth, mortality, or maturation. Across a range of temperatures, our
549 model predicted the benefits of growing large, including greater access to prey, greater
550 reproductive output per spawning event and lower risk of predation, outweighed the increased
551 metabolic costs. This approach can offer insight into nuanced variation in fish life histories
552 beyond covariance in growth and body size across large scales.
553
554 Although our approach is similar to prior models of life history traits grounded in energy
555 budgets, such as Dynamic Energy Budget Theory (Jusup et al 2011), we did not impose an
556 asymptotic function for growth in length or mass *a priori*. Physiological models broadly assume
557 that surface uptake areas relative to the volume of metabolically available mass leads to intrinsic
558 geometric constraints causing asymptotic growth (von Bertalanffy 1960, Pauly 2010). Instead,
559 multiple (mainly extrinsic) ecological mechanisms captured by our model led to slowing of
560 growth and emergence of an asymptotic size in each scenario. The availability of prey, limits on
561 resource intake, the risk of predation, and constraints on gonad size all increase the advantage of
562 growing to larger body sizes; these advantages are balanced against metabolic demands and the
563 actual energetic requirements of growth. Because the rate of mortality (Eq. 3) depends upon both
564 h and κ, in less productive ecosystems, individuals have lower risk of predation. Smaller

565 individuals also need fewer resources for metabolic maintenance but were predicted to have very
566 low lifetime reproductive output by comparison. Body sizes were predicted to be smaller in
567 warmer environments, all else being equal, but these effects were only pronounced at large
568 increases in temperatures (greater than 10 degrees Celsius; Figure 5A). In these dramatically
569 warmer scenarios, individuals were predicted to reduce reproductive output rather than growth
570 (Figure 5B). This trend of reduced reproduction increased in productive ecosystems, where
571 individuals were largest. Smaller temperature increases (five degrees C) had only minor effects,
572 suggesting that changes in resources, not direct responses to temperature, are likely mechansism
573 driving observed changes in fish growth patterns (e.g., Oke et al. 2020).
574
575 *Predicting ecological lifestyles of tunas in different environmental conditions*
576 We predicted growth and reproductive patterns in tuna species that matched distinct ecological
577 lifestyles occurring in different environmental conditions. We were able to generate growth
578 curves that were consistent with the expected maximum body sizes of species in each ecological
579 lifestyle. However, we also discovered that seasonality in ecological productivity and
580 environmental temperature itself led to the evolution of a greater maximum body size (over 3 m)
581 than the body size that emerged under constant conditions of similar mean richness and
582 temperature. This suggests that migratory tuna species (exhibiting latitudinal or vertical
583 movements) with temporally limited spawning opportunities evolve larger body sizes so
584 individuals can maximize their uptake of resources during the non-spawning season and
585 minimize constraints on reproduction during the spawning season. This should be considered
586 when predicting the life history responses of fishes to changing environmental conditions. For
587 example, while polar oceans may increase in temperature, they will remain strongly seasonal.

This result is one of the novel predictions of our model that warrants further investigation; while there is increasing attention to latitudinal trends in physiological processes in terrestrial systems (Yanco et al. 2022), the role of seasonality in driving life history evolution is still poorly understood.

Our results were largely insensitive to our choices of parameters in the size spectrum aside from its intercept (κ). One exception came when estimating age-specific mortality, which was sensitive to our choice of the value representing variation due to predator satiation or efficiency in prey capture (*h,* Eq. 3). However, this process did not substantially change growth trajectories.

There are several reasons that larger body sizes were favored in ecosystems with higher productivity κ. Recall that in more productive ecosystems, there are both more prey and more predators. Larger individuals have more prey resources, and lower chances of predation. They also can take in more resources per month; because resource intake is restricted to 60% of an individual's mass, small individuals are less able to take advantage of a rich prey base. Although larger individuals have to pay higher metabolic costs, their mass-specific metabolic requirements decrease. Additionally, an individual's potential reproductive output per month (current fitness in Eq. 14) was constrained by the body cavity to be 20% of structural mass ($\varphi = 0.2$). Sensitivity analyses of the parameter φ, which determines the fraction of body mass that can be devoted to reproduction (Eq. 10), demonstrated that growing to larger maximum body sizes is more advantageous when this constraint is more stringent ($\varphi = 0.1$). By contrast, when it is less stringent ($\varphi = 0.3$), growth patterns and maximum size do not change, even when productivity κ varied (Supp. Fig. 5). From this pattern, we infer that when gonad capacity is constrained, it

can indirectly affect the optimal body size as well as the spawning potential of ectothermic vertebrates.

In conclusion, we found theoretical evidence that variation in ecosystem productivity, seasonality, and temperature interacted to determine optimal patterns of growth and reproductive allocation in fishes. This generates many avenues that can be explored in future work. In our model, temperature directly affected metabolic costs. In reality, temperature could causally alter size spectrum productivity. Understanding of this link is needed to understand how species will respond to different environmental changes and climate change scenarios. Finally, when predicting future growth patterns under projected changes in climate, multiple ecological and physiological factors are likely to play a greater role than temperature in determining emergent life histories.

Acknowledgements

This work was supported by NSF DEB-1556779 to HKK and NSF DEB 15-55729 and ONR N000141912494 to MM. CH is funded by Research England. NKD was supported by the Discovery and Accelerator grants from Natural Science and Engineering Research Council and the Canada Research Chair program. MJJJ was supported by "*la Caixa"* Foundation, under agreement Nº 847648. We thank J. A. Draghi for help troubleshooting the optimization.

Appendix. Optimization details.

Dynamic programming equations (Eq. 14) are constrained optimization algorithms with the purpose of determining the optimal set of behaviors or decisions that maximize a quantitative metric over time, such as lifetime expected reproductive success. A key property is that the decisions at one time affect the state variables at the next time. When solving Eq. 14, we consider how the allocation decisions an individual makes during one month of its life affect its future size, energetic reserves (lipid stores) and chances of survival, and find the set of allocation to growth and reproduction that maximizes its fitness in a given environment. We are able to calculate lifetime fitness by solving the equation using backwards iteration. By starting at $t = T - 1$, and assuming there is no possibility of future fitness (i.e., the second term of Eq. 14 is equal to zero for all possible values of length and lipid stores) we can populate the array with the fitness of all possible combinations of length, lipid stores, and allocation strategies at $t = T - 1$; this fitness will be the first term on the right side of Eq. 14. This process is repeated, working backwards, until $t = 1$. We can thereby determine the combination of g and r that maximizes both current fitness at t, and the fitness expected from $t + 1$ until T, given the chance of survival, length, and lipid stores (the future states in Eq. 12) resulting from that particular strategy. Solving Eq. 14 in this way produces an array storing the proportional allocation to growth and reproduction that leads to the highest lifetime fitness, for all possible combinations of size and lipid stores (l and s) for every month until the final time T.

Solving a dynamic programming equation with two state variables, such as Eq. 14, is computationally expensive, and we employed a number of techniques to make the iteration more efficient and to approximate a smooth fitness surface. First, we constrained the parameter space

that was evaluated. Specifically, we used an integer index I (with a maximum of I_{max}) to represent lipid stores s, converting the index to values in joules in the dynamic loop. We then related the range of s we explored to each value of l (because lipid stores are constrained by l), by setting

$$s = \frac{0.6 \cdot I^3 \rho a {l_{max}}^3}{{I_{max}}^3}$$

In other words, we adjusted the numerical step size for possible values of s to be finer for smaller individuals. Furthermore, we used linear interpolation of state values (Clark and Mangel 2000) when computing expected future fitness in Eq. 14 to minimize discontinuities on the fitness landscape arising from the integer index of energetic state. We did not interpolate length, since its unit (centimeters) was sufficiently fine-grained that there were minimal effects of discontinuities.

All programming was done using R 4.1.1 and all code and model outputs are available at https://github.com/hkindsvater/size-spectra-life-history. We ran the code to solve the Dynamic Programming Equation and simulate the individual life histories using Rscript commands from the Linux shell of a 2019 MacPro with 16 cores and 96 GB of RAM. Jobs were run in parallel and the runtime of each job was between 60 and 120 minutes. The results of each job are presented in the figures summarizing growth, reproduction, and survival data; these analyses and figures were produced in the Rstudio IDE.

References

Andersen, K. H. 2019. *Fish Ecology, Evolution, and Exploitation: A New Theoretical Synthesis.* Princeton University Press, Princeton.

Andersen, K. H., Jacobsen, N. S., Farnsworth, K. D., and J. Baum. 2016. The theoretical foundations for size spectrum models of fish communities. *Canadian Journal of Fisheries and Aquatic Sciences* 73:575–588.

Audzijonyte, A., Richards, S.A., Stuart-Smith, R.D., Pecl, G., Edgar, G.J., Barrett, N.S., Payne, N. and Blanchard, J.L., 2020. Fish body sizes change with temperature but not all species shrink with warming. *Nature Ecology & Evolution*. 4:809-814.

Audzijonyte, A. and Richards, S.A., 2018. The energetic cost of reproduction and its effect on optimal life-history strategies. *American Naturalist*. 192:E150-E162.

Barnes, W., Maxwell, D., Reuman, D.C., and Jennings, S., 2010. Global patterns in predator-prey size relationships reveal size dependency of trophic transfer efficiency. *Ecology* 91:222-232.

Benoît, E., and M. J. Rochet. 2004. A continuous model of biomass size spectra governed by predation and the effects of fishing on them. *Journal of Theoretical Biology* 226:9-21.

Bernal, D. 2011. Physiological specializations of different fish groups. Pelagic fishes. Pages 1887-1902 *in* Farrell AP (ed) *Encyclopedia of Fish Physiology: From Genome to Environment,* Vol 3. Academic Press, San Diego.

Bernal, D., Sepulveda C., Musyl, M., Brill, R. (2009) The eco- physiology of swimming and movement patterns of tunas, billfishes, and large pelagic sharks. Pages 436–483 *in* Domenici P, Kapoor BG (eds) *Fish Locomotion: an Etho-Ecological Approach*. Science Publishers, Enfield.

Bernal, D., Brill, R.W., Dickson, K.A. and H.A. Shiels. 2017. Sharing the water column: physiological mechanisms underlying species-specific habitat use in tunas. *Reviews in Fish Biology and Fisheries* 27:843-880.

Bernhardt, J.R., Sunday, J.M. and M.I. O'Connor. 2018. Metabolic theory and the temperature-size rule explain the temperature dependence of population carrying capacity. *American Naturalist.* 192:687-697.

Beverton, R. J. H., and S. J. Holt. 1959. A review of the lifespans and mortality rates of fish in nature, and their relation to growth and other physiological characteristics. Pages 142–177 *in* CIBA Foundation Colloquium on Ageing.

Bigman, J.S., M'Gonigle, L., Wegner, N.C. and Dulvy, N.K. 2021. Respiratory capacity is twice as important as temperature in driving patterns of metabolic rate across the vertebrate tree of life. *Science Advances* 7: eabe5163.

Blanchard, J. L., Heneghan, R. F., Everett, J. D. , Trebilco, R. and A. J. Richardson. 2017. From bacteria to whales: using functional size spectra to model marine ecosystems. *Trends in Ecology & Evolution.* 32:174-186.

Blanchard, J. L., Jennings, S., Law, R., Castle, M.D., McCloghrie, P., Rochet, M.J., and E. Benoît. 2009. How does abundance scale with body size in coupled size-structured food webs? *Journal of Animal Ecology*. 78:270-280.

Blanchard, J.L., Jennings, S., Holmes, R., Harle, J., Merino, G., Allen, J.I., Holt, J., Dulvy, N.K. and M. Barange. 2012. Potential consequences of climate change for primary production and fish production in large marine ecosystems. *Phil. Trans. Roy. Soc. B* 367:2979-2989.

Brown, J. H., J. F. Gillooly, A. P. Allen, V. M. Savage, and G. B. West. 2004. Toward a metabolic theory of ecology. *Ecology.* 85:1771-1789.

Chapman, E. W., Kørgensen, C., and M. E. Lutcavage. 2011. Atlantic bluefin tuna (*Thunnus thynnus*): a state-dependent energy allocation model for growth, maturation, and reproductive investment. *Canadian Journal of Fisheries and Aquatic Sciences* 68:1934–1951.

Charnov, E. L., Berrigan, D., and R. J. H. Beverton. 1991. Dimensionless numbers and the assembly rules for life histories. *Phil. Trans. Roy. Soc. B* 332:41-48.

Charnov, E. L., and J. R. Krebs. 1974. On clutch-size and fitness. *Ibis.* 116:217-219.

Cheung, W.W., Close, C., Lam, V., Watson, R., and D. Pauly 2008. Application of macroecological theory to predict effects of climate change on global fisheries potential. *Marine Ecology Progress Series*. 365:187-197.

Clark, C. W., and M. Mangel. 2000. Dynamic state variable models in ecology: methods and applications. Oxford University Press, Oxford.

Clarke, A. 2006. Temperature and the metabolic theory of ecology. *Functional Ecology* 20:405-412.

Clarke, A., and N. M. Johnston. 1999. Scaling of metabolic rate with body mass and temperature in teleost fish. *Journal of Animal Ecology*. 68: 893-905.

Conover, D. O., and S. B. Munch. 2002. Sustaining fisheries yields over evolutionary timescales. *Science* 297:94–96.

Daufresne, M., Lengfellner, K., and U. Sommer. 2009. Global warming benefits the small in aquatic ecosystems. *Proc. Nat. Acad. Sci.* 106:12788–12793.

Dickson, K.A., and Graham, J.B. 2004. Evolution and consequences of endothermy in fishes *Physiological and Biochemical Zoology* 77: 998-1018.

Fernandes, J.A., Rutterford, L., Simpson, S.D., Butenschön, M., Frölicher, T.L., Yool, A., Cheung, W.W. and Grant, A., 2020. Can we project changes in fish abundance and distribution in response to climate? *Global Change Biology.* 26:3891-3905.

Free, C.M., Thorson, J.T., Pinsky, M.L., Oken, K.L., Wiedenmann, J. and Jensen, O.P. 2019. Impacts of historical warming on marine fisheries production. *Science.* 363: 979-983.

Froese R. 2006. Cube law, condition factor and weight-length relationships: history, meta-analysis and recommendations. *Journal of Applied Ichthyology* 22: 241-253

Gadgil, M., and W. H. Bossert. 1970. Life historical consequences of natural selection. *American Naturalist* 104:1-24.

Gillooly, J. F., Brown, J. H., West, G. B., Savage, V. M., and E. L. Charnov. 2001. Effects of size and temperature on metabolic rate. *Science.* 293:2248–2251.

Gislason, H., Daan, N. Rice, J. C., and J. G. Pope. 2010. Size, growth, temperature and the natural mortality of marine fish. *Fish and Fisheries* 11:149–158.

Hilborn, R. and Mangel, M. 1997. *The Ecological Detective.* Princeton University Presson, Princeton, NJ.

Horswill, C., H. K. Kindsvater, M. J. Juan-Jordá, N. K. Dulvy, M. Mangel, and J. Matthiopoulos. 2019. Global reconstruction of life-history strategies: A case study using tunas. *Journal of Applied Ecology* 56:855-865.

Houston, A., C. Clark, J. McNamara, and M. Mangel. 1988. Dynamic Models in Behavioural and Evolutionary Ecology. *Nature.* 332:29-34

Houston, A., and J. McNamara. 1999. *Models of Adaptive Behaviour*. Cambridge University Press.

Jørgensen, C., K. Enberg, and M. Mangel. 2016. Modelling and interpreting fish bioenergetics: a role for behaviour, life-history traits and survival trade-offs. *Journal of Fish Biology* 88:389–402.

Jørgensen, C., and Ø. Fiksen. 2006. State-dependent energy allocation in cod (*Gadus morhua*). *Canadian Journal of Fisheries and Aquatic Sciences* 63:186–199.

Juan-Jordá, M. J., I. Mosqueira, J. Freire, and N. K. Dulvy. 2013. The Conservation and Management of Tunas and Their Relatives: Setting Life History Research Priorities. *PLoS ONE 8:e70405.*

Jusup, M., Klanjscek, T., Matsuda, H., Kooijman, S.A.L.M. 2011. A Full Lifecycle Bioenergetic Model for Bluefin Tuna. *PLoS ONE* 6(7): e21903.

Kindsvater, H.K., Alonzo, S.H., Mangel, M. and Bonsall, M.B., 2010. Effects of age-and state-dependent allocation on offspring size and number. *Evolutionary Ecology Research*, 12(3), pp.327-346.

Kingsolver, J. G., and R. B. Huey. 2008. Size , temperature , and fitness : three rules. *Evolutionary Ecology Research* 10:251–268.

Kiørboe, T., and A. G. Hirst. 2014. Shifts in mass scaling of respiration, feeding, and growth rates across life-form transitions in marine pelagic organisms. *American Naturalist* 183:E118-E130.

Kitchell, J.F., Neill, W.H., Dizon, A.E., and J.J. Magnuson. 1978. Bioenergetic Spectra of Skipjack and Yellofin Tunas. In:Sharp, G.D., Dizon, A.A. (Eds.), *The Physiological Ecology of Tunas.* Academic Press.

Kozlowski, J. 1996. Optimal allocation of resources explains interspecific life-history patterns in animals with indeterminate growth *Proc. R. Soc. B.* 263:559-566.

Law, R., M. J. Plank, A. James, and J. L. Blanchard. 2009. Size-spectra dynamics from stochastic predation and growth of individuals. *Ecology* 90:802-811.

Oke, K.B., Cunningham, C.J., Westley, P.A.H., Baskett, M.L., Carlson, S.M., Clark, J., Hendry, A.P., Karatayev, V.A., Kendall, N.W., Kibele, J. ,Kindsvater, H.K., Kobayashi, K.M., Lewis, B., Munch, S., Reynolds, J.D., Vick, G.D., and E.P. Palkovacs. 2020. Recent declines in salmon body size impact ecosystems and fisheries. *Nature communications*, 11:1-13.

Mangel, M. 2006. The Theoretical Biologist's Toolbox : Quantitative Methods for Ecology and Evolutionary Biology. Cambridge University Press.

Mangel, M. 2015. Stochastic dynamic programming illuminates the link between environment, physiology, and evolution. *Bulletin of Mathematical Biology* 77:857-877.

Mangel, M. and C. W. Clark. 1988. *Dynamic Modelling in Behavioral Ecology.* Princeton University Press, Princeton.

Monsch, K.A. 2000 *The Phylogeny of the Scombroid Fishes.* PhD thesis, University of Bristol p 272.

Neubauer, P., and K. H. Andersen. 2019. Thermal performance of fish is explained by an interplay between physiology, behaviour and ecology. *Conservation Physiology* 7:coz025

Pauly D. 2010. Gasping fish and panting squids: oxygen, temperature and the growth of water-breathing animals. International Ecology Institute, Germany.

Pilakouta, N, Killen, SS, Kristjánsson, BK, et al. 2020. Multigenerational exposure to elevated temperatures leads to a reduction in standard metabolic rate in the wild. *Funct Ecol*. 34:1205-1214.

Pignalosa, P., Pappalardo, L., Gioacchini, G., Carnevali, O. 2020. Length-weight relationships and a new length conversion factor for Atlantic Bluefin tuna (*Thunnus thynnus L.*) caught in the Mediterranean Sea. *Collect. Vol. Sci. Pap. ICCAT,* 76(2): 138-146.

Schaefer, K.M. 2001. Reproductive biology of tunas. *Fish Physiology.* 19: 225-270.

Schaefer K.M., Fuller D.W., and B.A. Block 2009. Vertical movements and habitat utilization of skipjack (*Katsuwonus pelamis*), yellowfin (*Thunnus albacares*), and bigeye (*Thunnus obesus*) tunas in the Equatorial Eastern Pacific Ocean, ascertained through archival tag data. Pages 121-144 *in* Nielsen, J.L., Arrizabalaga, H., Fragoso, N., Hobday, A., Lutcavage, M., Sibert, J. (Eds.), *Tagging and Tracking of Marine Animals with Electronic Devices*. Springer, New York.

Sheldon, R.W., Prakash, A. and Sutcliffe Jr., W.H. 1972. The distribution of particles in the ocean. *Limnology and Oceanography.* 17:327-340.

Sheldon, R.W., Sutcliffe Jr., W.H., and M.A. Paranjape. 1977. Structure of pelagic food chain and relationship between plankton and fish production. *Journal of the Fisheries Research Board of Canada*. 34: 2344-2353.

Southwood, T.R.E. 1977. Habitat, the Templet for Ecological Strategies? *Journal of Animal Ecology*. 46:337-365.

Sprules, W. G., and L. E. Barth. 2016. Surfing the biomass size spectrum: some remarks on history, theory, and application. *Canadian Journal of Fisheries and Aquatic Sciences* 73:477-495.

Thygesen, U.H., Farnsworth, K.D., Andersen, K.H., Beyer, J.E. 2005. How optimal life history changes with the community size-spectrum. *Proc. R. Soc. B*. 272:1323-1331.

Trebilco, R., Baum, J. K., Salomon, A. K., and N. K. Dulvy. 2013. Ecosystem ecology: Size-based constraints on the pyramids of life. *Trends in Ecology & Evolution*. 28:423-431.

Ursin, E. 1973. On the prey size preferences of cod and dab. *Meddelelser fra Danmarks Fiskeri- og Havundersøgelser* 7: 85–98.

Varpe, O. 2017 Life history adaptations to seasonality, *Integrative and Comparative Biology*, **57:** 943–960.

von Bertalanffy L. 1960. Principles and theory of growth. Pages 137-259 *in* Nowinski, W.W., Ed., *Fundamental Aspects of Normal and Malignant Growth*, Elsevier, Amsterdam.

Walsh, M. R., and D. N. Reznick. 2009. Phenotypic diversification across an environmental gradient: a role for predators and resource availability on the evolution of life histories. *Evolution* 63:3201–3213.

Wong, S., Bigman, J.S., and N.K. Dulvy. 2021. The metabolic pace of life histories across fishes. *Proc. R. Soc. B*. 288:20210910.

Wootton, H.F., Morrongiello, J.R., Schmitt, T. & Audzijonyte, A. 2022. Smaller adult fish size in warmer water is not explained by elevated metabolism. Ecology Letters, 25, 1177– 1188.

Yanco, S.W., Pierce, A.K. and Wunder, M.B. 2022. Life history diversity in terrestrial animals is associated with metabolic response to seasonally fluctuating resources. Ecography. 2022:e05900

Table 1. Description of parameters and variables

Parameter or Variable	Description	Value
w	Body mass in kg	varies
B	Absolute biomass in a trophic level (prey or predators) when considering a community size spectrum	-
κ	The intercept of a biomass size spectrum, which defines the total biomass of organisms of the smallest body size w in a given ecosystem; Andersen (2019) gives an estimate of 10 gained by averaging over all Predator-Prey Mass Ratio estimates measured from gut contents. We vary it to represent ecosystem differences in overall ecosystem richness	1, 2.5, 5
$Bprey$	Biomass of prey expected by a focal individual	-
μ_p	Instantaneous risk of mortality due to predation, which depends on body mass and position in the size spectrum	-
h	Predation risk, comprised of predator satiation estimates (estimated from gut contents) and predator preference (or effectiveness) for consuming prey of a given mass (Andersen 2019)	4, 8
τ	Temperature of the environment (in degrees Kelvin)	285-300
C	Metabolic requirements (costs) that scale with mass and temperature	-
c	Normalization constant scaling metabolic costs (in J), based on metabolic rate data from tunas (Kitchell et al. 1978)	5×10^{16}
k_B	Boltzmann constant, relating particle energy to temperature in units of m^2 kg s^{-2} K^{-1}	1.3×10^{-23}
E	The average activation energy for the rate limiting enzymes in metabolism in units of joules; from the metabolic theory of ecology (Gillooly et al. 2001).	1.04×10^{-19}
θ	Metabolic scaling exponent; values vary among clade, here we use a value reported for tunas (Clarke and Johnston 1999)	0.66
ρ	The energy density of tuna body mass in our model in J/kg (estimated empirically and reported in Chapman et al. 2011)	4.2×10^{6}
t	Time in monthly time steps in the dynamic model	-
T_{max}	Maximum lifespan in months	216
l, $L(t)$	Body length (in cm) This is a dynamic state variable but can only increase with time. The maximum value possible is 400 cm. For a specific value, we use the capital letter notation.	-
s, $S(t)$	Lipid stores (in joules) – this is a dynamic state variable representing energy stores that can be used for metabolism, growth, and reproduction.	-
a	Scale coefficient relating length to structural mass, similar to values estimated empirically for bluefin tuna and reported in Pignalosa et al. (2020).	1.0×10^{-5}
$w(t)$	Structural mass of the individual (in kg) at time t – this depends on $L(t)$	-
υ	The fraction of structural mass that determines the critical threshold of energetic mass needed for survival	0.1
φ	The fraction of structural mass that determines the maximum limit on reproductive output in a monthly time step	0.2
γ_{pred}	Survival from predation from one month to the next	
γ_s	Survival, given that the individual has sufficient energy reserves to meet metabolic requirements and avoid starvation	
g	Proportion of lipid stores allocated to growth (this allocation decision is optimized by the dynamic programming equation); can take values between 0 and 1	
r	Proportion of lipid stores allocated to reproduction (this allocation decision is optimized by the dynamic programming equation); can take values between 0 and 1 and the sum of g and r cannot exceed one.	
$R(l,s,t)$	Current fitness, the product of lipid stores and the optimal allocation to reproduction, r	
$V(l,s,t)$	Expected accumulated lifetime reproduction from time t onwards, given that $L(t) = l$ and $S(t) = s$	

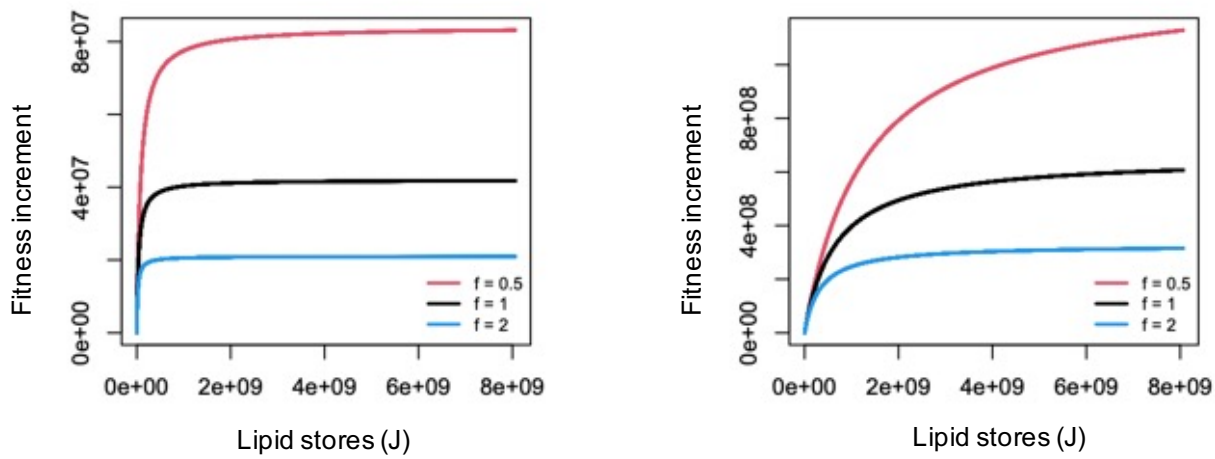

Supplementary Figure 1. The fitness increment expected with different amounts of energy reserves (lipid stores) (A) for an individual of length 100 cm and (B) an individual of length 250 cm. We show the shape of the curve for three values of f, but for all analyses presented here we use $f = 1$.

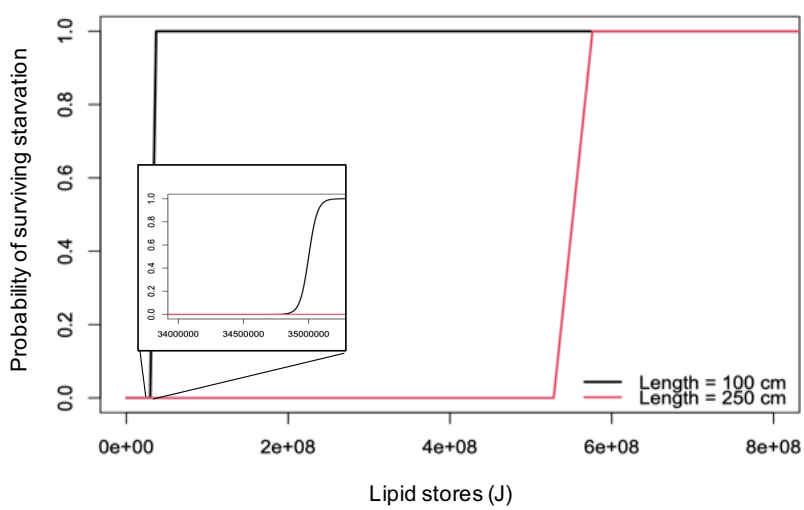

Supplementary Figure 2. Main panel: The sigmoid relationship between lipid stores (in joules) and survival for individuals of different lengths. The threshold amount of energy required for metabolic maintenance is a fixed proportion of body mass. The probability of avoiding starvation $\gamma_s(s, l)$ is a logistic function of mass given in Eq. 13. Inset: closeup of the x-axis in the region encompassing the smaller threshold.

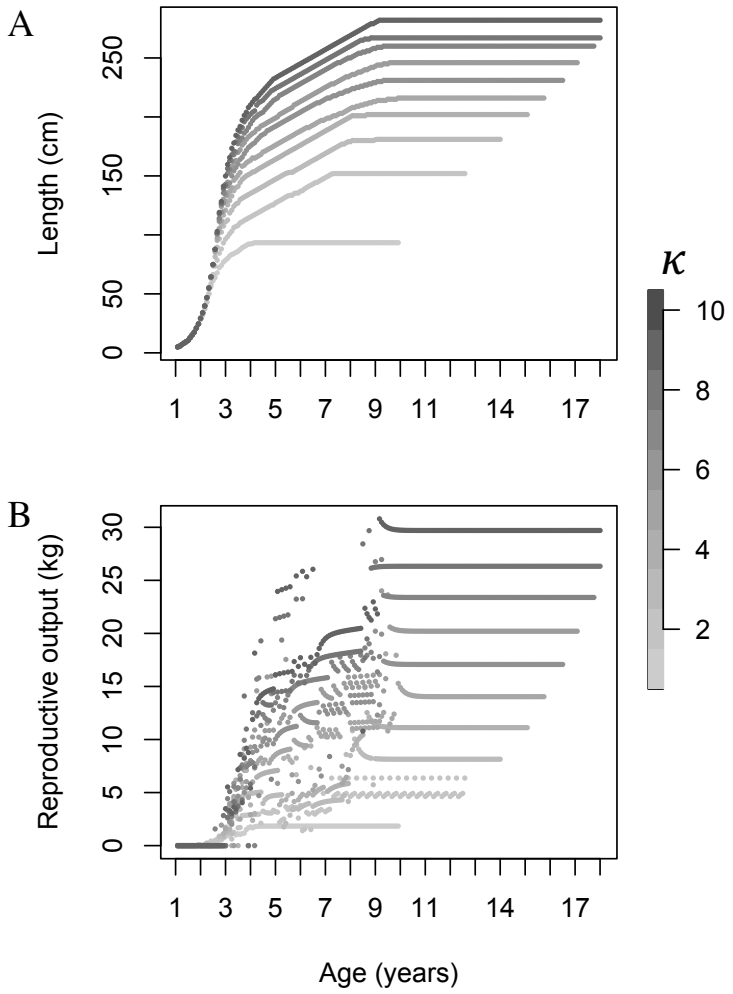

Supplementary Figure 3. Alternate version of main text Figure 5 showing the discontinuous results predicted in our forward simulation, which are a result of the discrete steps necessary in our numeric optimization. The curves in (B) are more disjunct than (A) because, unlike length, reproductive output is not cumulative.

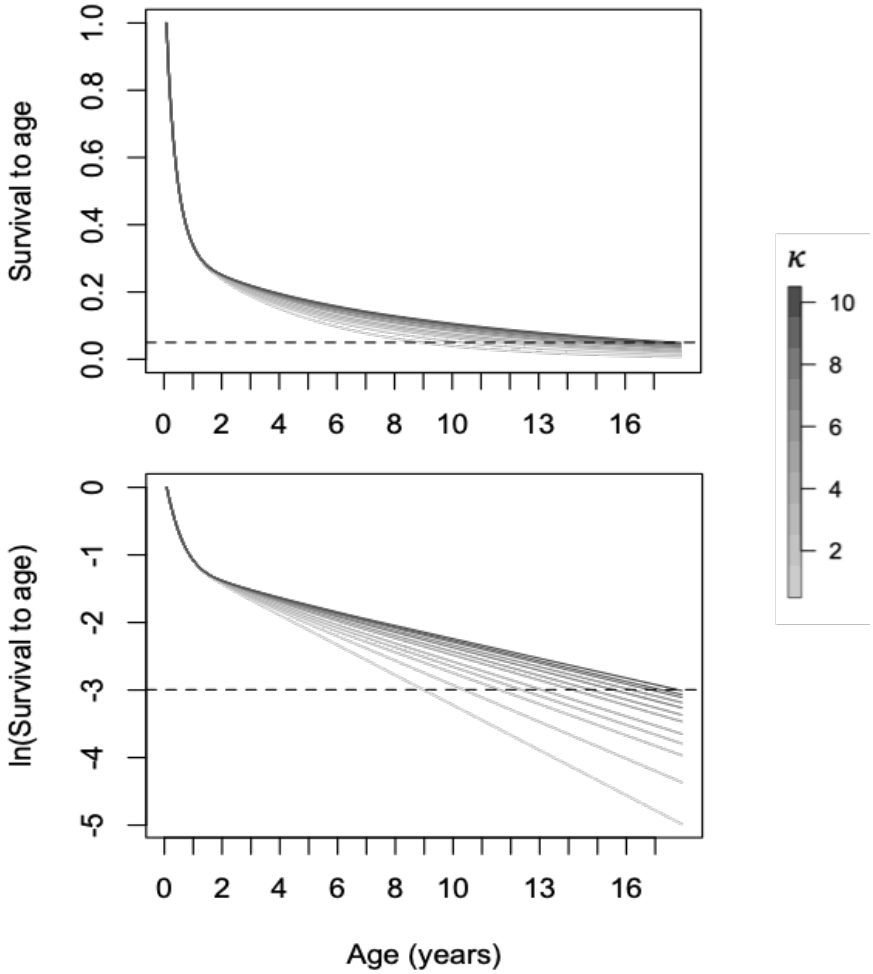

Supplementary Figure 4. Top: The emergent pattern of survival to age at different levels of κ. Bottom: The natural log of survival to age. Dashed horizonal line shows the cutoff past which less than 5% of individuals will survive. For all results here, $h = 8$ and $\tau = 16.85$ C.

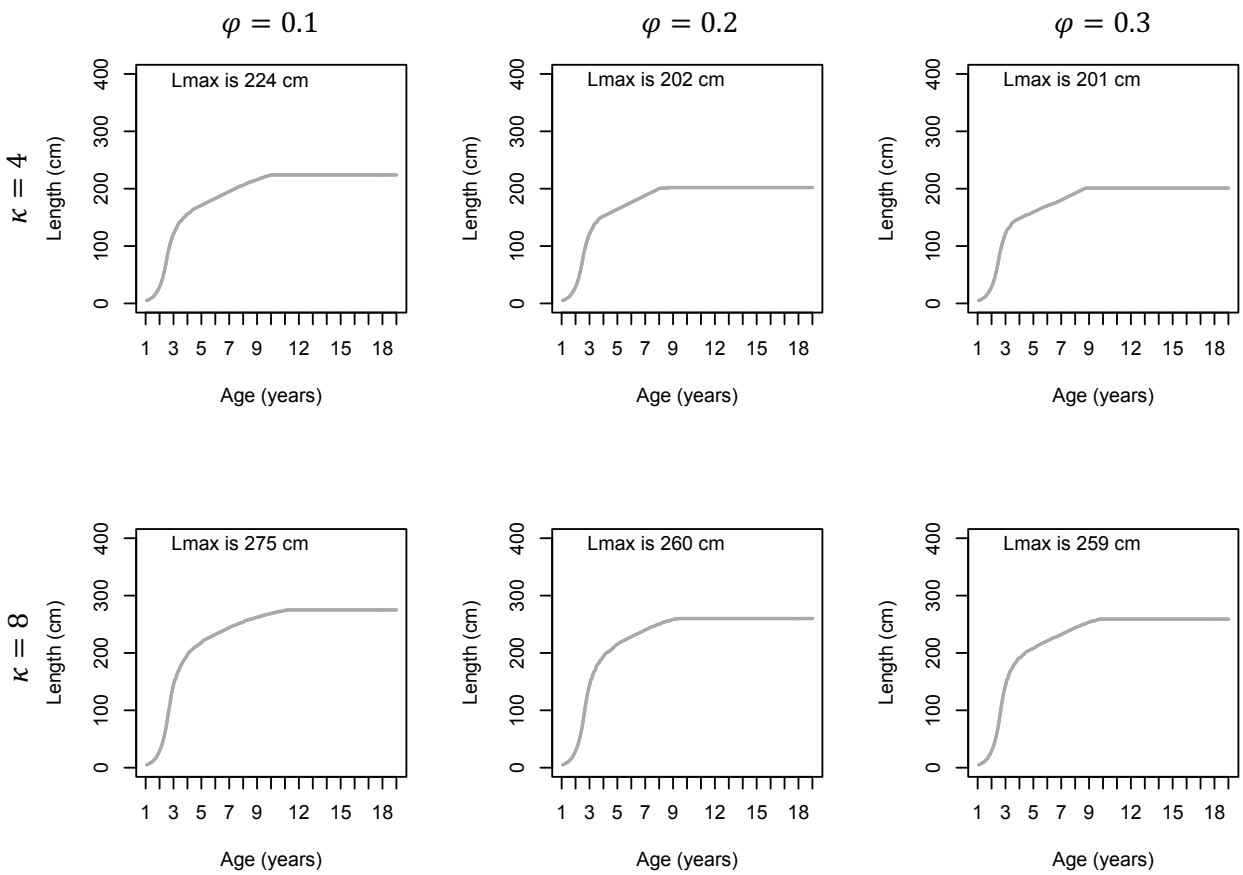

Supplementary Figure 5. Growth curves showing the effect of changes in the reproductive capacity φ (columns), for two intermediate values of κ (rows). As the reproductive constraint increases (the fraction of the body cavity that can be devoted to gonad decreases from 0.2 to 0.1), selection favors the evolution of larger body sizes. By contrast, there is little difference between 0.2 and 0.3 for both productivity scenarios. In all scenarios, $\tau = 16.85$C. Note that for all results presented elsewhere, $\varphi = 0.2$.

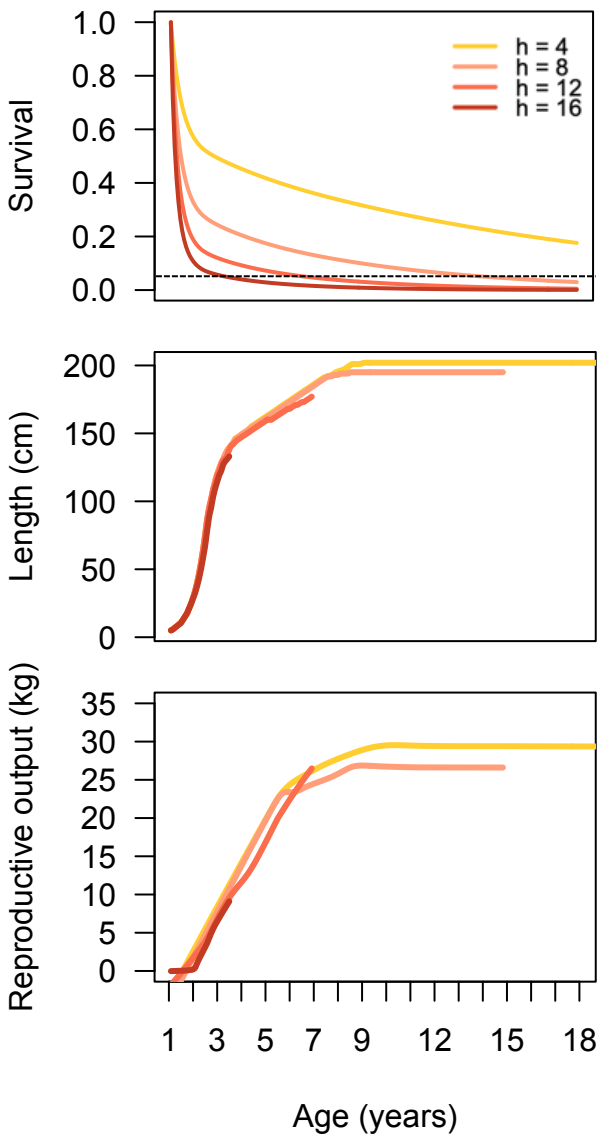

Supplementary Figure 6. The emergent patterns of age-specific survival, growth, and reproduction that emerges when h varies. For all results here, $\kappa = 4$ and $\tau = 16.85$C. Note that for all results presented elsewhere, $h = 8$. The dashed black line represents the 5% survival cutoff used throughout to establish average lifespan. Note that for $h = 4$ survival at $T = 18$ is well above 5% so these individuals live past the model timeframe.

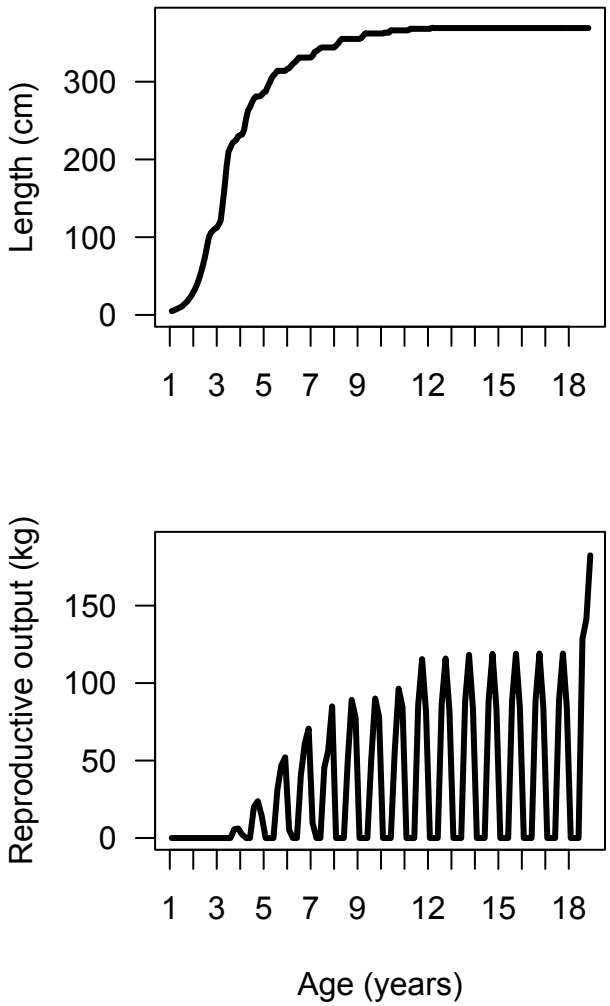

Supplementary Figure 7. Growth (top) and reproduction (bottom) predicted in ecosystems corresponding to seasonal conditions where individuals migrate from productive waters to warmer waters. Conditions are identical to the temperate deep-diving lifestyles in Fig 7C, F. The key difference is in duration of foraging and spawning seasons. In this scenario, individuals spend half the year in cool, productive foraging grounds and the other half in warm, resource-poor environments, instead of nine months foraging and three months on the spawning grounds as in Fig. 7C, F.

961